



An Overview of Improvements to the COS FUV Geometric Distortion and Walk Corrections

Nick Indriolo^{1,2}, T. Ake¹, J. Debes^{1,2}, D. French¹, S. Hasselquist¹, D. Kakkad^{1,3}, M. Rafelski¹, D. Sahnou¹, G. De Rosa¹, W. Fischer¹, E. Frazer¹, R. Plesha¹, C. Proffitt¹, J. Roman-Duval¹

¹ Space Telescope Science Institute, Baltimore, MD

² AURA for European Space Agency, STScI, USA

³ Centre for Astrophysics Research, University of Hertfordshire, Hatfield AL10 9AB, UK

2 July 2025

ABSTRACT

The process of assigning incident photons to digital pixels on the far ultraviolet (FUV) detector of the Cosmic Origins Spectrograph (COS) suffers from distortions. Nominally these are removed via the geometric distortion correction and walk correction steps within the CalCOS pipeline, but over time it has become apparent that at some locations on the detector the existing corrections are inadequate. Here we describe the overall effort to revise the COS FUV geometric distortion and walk corrections, first explaining the need for new corrections, and then presenting results that demonstrate improved calibration.

Contents

1. Introduction	2
2. Motivations	4
3. Procedures	7

3.1 Testing Metrics	7
3.2 Workflow	8
3.3 Geometric Distortion Measurement	9
3.4 X-Walk Measurement	9
3.5 Y-Walk Measurement	10
3.6 Delta Geometric Distortion Correction	10
4. Summary	11
5. Future Work	13
Acknowledgements	14
Change History for COS ISR 2025-07	14
References	17

1. Introduction

Two of the early steps in the processing of Cosmic Origins Spectrograph (COS) far ultraviolet (FUV) observations are the geometric distortion correction and walk correction. Roughly speaking, the purpose of these corrections is to take the raw, distorted image returned by the detector and to move photon events so that the resulting image has a rectilinear format with uniform pixel size and no gain dependence. To understand why such corrections are necessary, a brief description of how the COS FUV detector operates is required.

The COS FUV detector does not have physical pixels. A photon incident upon a detector segment impacts the photocathode layer at the top of the microchannel plate (MCP) stack, liberating an electron that the MCP stack amplifies. This creates a charge cloud on the anode beneath the MCP, which sends electronic pulses in both directions down two cross-delay lines (one in x , one in y). The difference in arrival time of the pulses at the ends of one delay line specifies the location of the incident photon along that axis. Based on this timing difference, each photon is assigned to a digital pixel in an array of size 16384×1024 ($x \times y$). These correspond to the RAWX and RAWY coordinates that appear in COS photon event lists.¹ The details of this assignment were fine-tuned before launch, and correspond to pixels that are approximately $6 \mu\text{m}$ wide and $24 \mu\text{m}$ high. For each detector segment the full digital pixel grid corresponds to a physical region that is larger in extent than the physical area of the segment that is sensitive to incident photons. The region that is responsive to photons, known as the active area, extends about 14000 pixels in the x -direction and about 400 pixels in the y -direction on both detector segments, although the exact location in the digital pixel grid differs for the two segments (for a visual representation see Figures 4.1 and 4.6 in the COS Instrument Handbook; Hirschauer et al. 2024).

While assigning location based on timing difference is conceptually simple, in practice there are multiple effects that make this process more complicated. First,

¹Note that the x -axis used by the detector is reversed with respect to the x -axis provided to users in data files, and that strictly speaking $\text{RAWX} = 16383 - x_{\text{detector}}$

the speed of the electronic pulses down the delay line has a temperature dependence (Wilkinson et al. 2001). Within CalCOS—the standard calibration pipeline for COS data—this is addressed by the thermal distortion correction, TEMPCORR, which we will not discuss further here². Second, each electronic pulse has a finite width and amplitude, so measuring the time at which a pulse arrives at the end of the delay line is a non-trivial matter. The signal processing that goes into measuring the pulse arrival time was designed to eliminate any dependence on pulse amplitude, but not on pulse width (Vallerga & McPhate 2000). Because the width of a pulse increases as it travels down the delay line, the pulse width at the end of the line varies as a function of the incident photon location. This effect, coupled with signal reflections that occur within the electronics, makes it so that the pulse arrival time is not always measured from the exact same location within a pulse. Additionally, localized variations in the properties of the anode substrate cause differences in the pulse propagation speed so that the relationship between location and pulse travel time is not quite linear. The end result of these timing inaccuracies is that the digital pixels in different locations on the detector correspond to slightly different physical sizes. This is known as integral non-linearity and is what we refer to as the geometric distortion (Vallerga et al. 2001; Wilkinson et al. 2001). The purpose of the geometric distortion correction (GEOCORR) is to reassign the pixel coordinates for every photon event, moving them from this non-uniform pixel array to a new pixel array where all pixels correspond to the same physical size on the detector ($6 \times 24 \mu\text{m}$).

Walk is also related to pulse-timing inaccuracies, but in this case depends on the gain of the detector (total charge received at the anode per incident photon). The gain of each COS FUV photon event is encoded in a 5-bit number (i.e., 0–31) known as the pulse-height amplitude (PHA). The size of the charge cloud on the anode produced by a single photon varies as a function of the detector gain, resulting in different pulse heights and widths. Because the detector electronics were optimized to record photon location at a specific gain, at other gain levels the different pulse widths cause photons that impact the same location on the detector to be assigned to different digital pixels (i.e., “walking”). This shift as a function of gain is assumed to operate independently in the x and y directions, with the shift in x also having an x -dependence and the shift in y also having a y -dependence. The purpose of the walk corrections (XWLKCORR and YWLKCORR) is to shift all photon events into the reference frame defined by a single gain level.

To summarize, starting from the initially assigned digital pixels (RAWX,RAWY), each photon event is corrected for thermal distortions (TEMPCORR), moved to a new array of uniformly sized (in physical space) digital pixels (GEOCORR), and shifted to align events at different PHA (XWLKCORR and YWLKCORR). Upon completion of these calibration steps, photon events are in the (XCORR,YCORR) coordinate frame upon which all further data processing depends. In this document, we present an overview of improvements made to the latter two steps

²For a detailed description of TEMPCORR, see the COS Data Handbook; Soderblom et al. (2022)

(i.e., geometric distortion correction and walk correction) via the analysis of several different data sets and updates to the GEOFILE, DGEOFILE, XWLKFILE, and YWLKFILE reference files. Detailed discussions of these analyses can be found in the following documents: Kakkad et al. (2025)—geometric distortion correction; Indriolo et al. (2025a)—delta-geometric correction; Hasselquist et al. (2025a)—X-walk correction; Hasselquist et al. (2025b)—Y-walk correction; French et al. (2025)—development of testing metrics.

2. Motivations

The existing³ geometric distortion correction for the COS FUV detector has been applied to on-orbit data since 2009, when the instrument was installed on the *Hubble Space Telescope* (HST). At that time, spectra were projected onto the center of the FUV detector in the cross-dispersion direction at what is now referred to as the first lifetime position (LP1). Repeated observations at the same location on the detector cause a drop in sensitivity to incident photons known as gain sag, and the default location in the cross-dispersion direction where spectra are recorded has been shifted over time to mitigate this effect. As of June 2025, a majority of COS FUV observations are taken at LPs that are about ± 5 arcsec (± 60 pixels) off of the central axis where LP1 is located. While the geometric distortion correction at LP1 was well-vetted, it has become apparent over time that the off-axis correction suffers from systematic errors that introduce artifacts into processed data. For example, an analysis of wavelength residuals on the short-wavelength side of the FUV segment at LP4 (5 arcsec below LP1) reveals that deviations from a linear dispersion solution are caused by rapid variations in the dx geometric distortion correction (see Figure 1). Similarly, the grid wire “impostors” (Osten et al. 2013) near both edges of the FUVB segment—regions of decreased flux that are currently fixed in the flat field calibration step—are again due to rapid variation in the dx geometric distortion correction (see Figure 2). By revisiting and improving the geometric distortion correction, we aim to remove these errors from calibrated COS FUV data.

While operating at a single lifetime position and high voltage level, the modal gain at that location steadily drops with use, introducing increasingly larger walk. The effects of Y-walk (distortions to the spectral trace in cross-dispersion direction; see Figure 4.5 in Hirschauer et al. 2024) became clear early on in the operational lifetime of COS, and so a Y-walk correction was implemented. The magnitude of this shift (dy as a function of PHA) was measured at a single location on FUVB at LP1, and the correction derived from this analysis has been applied to all COS data since then (Sahnou et al. 2011). However, it was recently found that the dy vs. PHA relationship varies as a function of YCORR, and applying a single correction everywhere on the detector can move photons

³Throughout this document, the “existing” reference file refers to the version with known issues that motivated the project described herein, and is used interchangeably with “old” version.

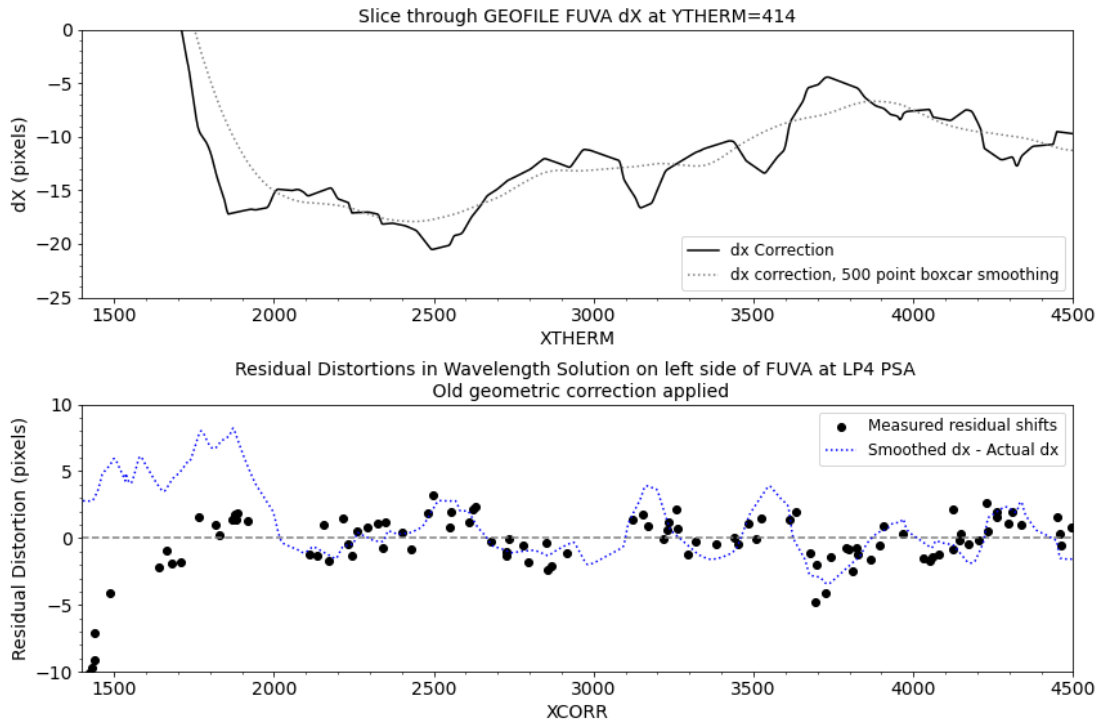


Figure 1. The top panel shows a slice through the old (`x1u1459gl_geo.fits`) FUVA dx geometric distortion correction at YTHERM=414 (LP4 location) in solid black, and a 500 point boxcar average of the same correction in dotted grey. XTHERM and YTHERM refer to the thermally corrected reference frame (after application of TEMPCORR), the coordinate system in which the geometric distortion correction is defined. The bottom panel shows the residual shifts (in pixels) between the measured and predicted locations for emission lines in the spectrum of ϵ Eri observed on the left side of FUVA at LP4 for data processed with the old geometric distortion correction as black circles. The dotted blue curve is the difference between the smoothed and actual curves in the top panel (note that this curve has been shifted from XTHERM to XCORR coordinates). There is a clear correlation between the difference curve and data points, with larger residuals found at locations where the dx correction rapidly deviates from the average correction. This is evidence that the geometric distortion correction is *introducing* artifacts in the calibrated data.

out of the spectral extraction region (see Figure 3). To improve upon the existing Y-walk correction, we will measure the shift as a function of PHA and YCORR on both detector segments and apply a new y-dependent correction.

This drop in modal gain also affects the walk in the dispersion (x) direction. Observations were designed and executed to measure the magnitude of this X-walk (HST program 12793; PI: G. Kriss) and preliminary analyses of these data were reported by Sahnou et al. (2016) and Sahnou (2018). They found that the magnitude and

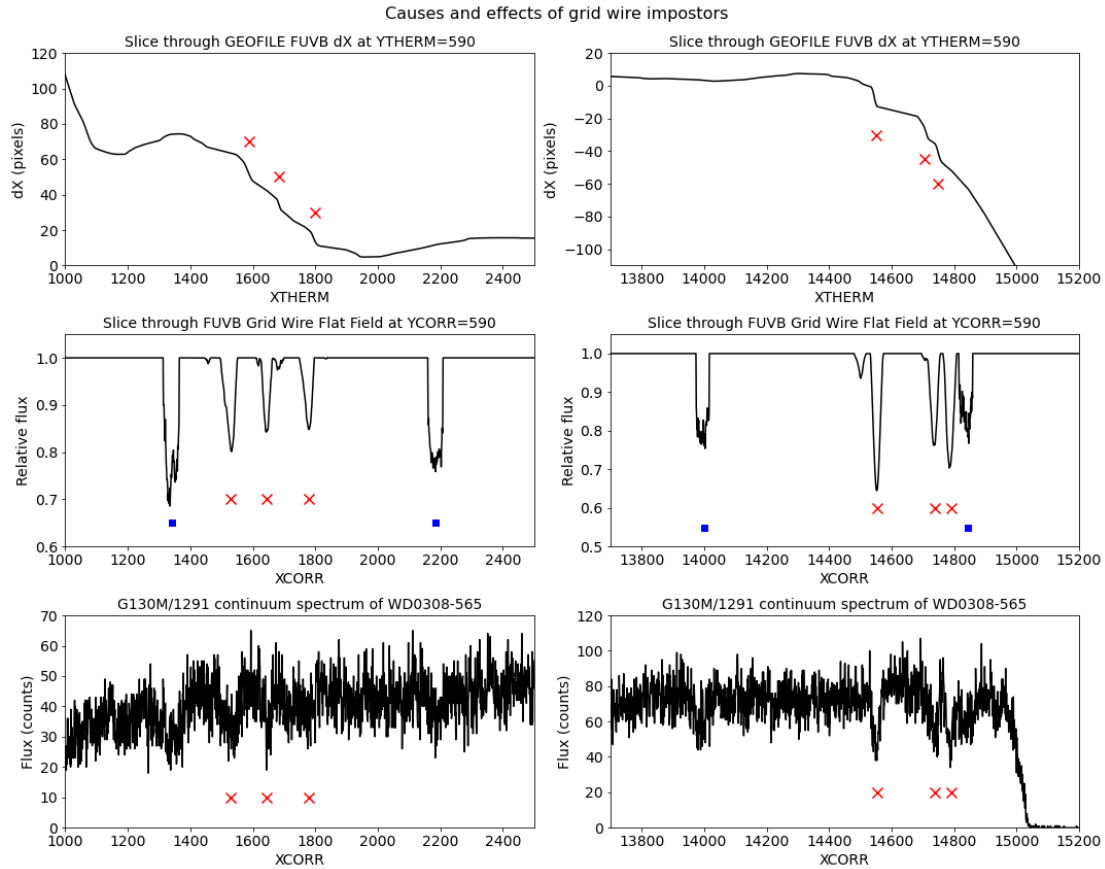


Figure 2. From top to bottom these panels show: (1) a slice through the existing (`x1u1459gl_geo.fits`) FUVB dx geometric distortion correction; (2) a slice through the FUVB grid wire flat field; (3) a continuum spectrum without the flat field correction applied (i.e., `FLATCORR=OMIT`). In the middle two panels red crosses mark the grid wire impostors, while blue squares mark the actual grid wire shadows. In the bottom panels the red crosses mark the reduced flux caused by the grid wire impostors. Note that the reduced flux caused by the grid wire impostors is accounted for in the L-flats, so in fully calibrated FUV data these features are removed. The flat correction has not been applied here to demonstrate the effects that these features have on spectra. In the top panels the red crosses mark the rapid changes in the dx correction that give rise to the grid wire impostors. The problem arises because the flux on a small portion of the detector is smeared out across too many pixels, resulting in an artificial flux deficit.

direction of X-walk depends both on PHA and XCORR, and that in some locations on the detector errors induced by X-walk can exceed the six-pixel size of a resolution element in the dispersion direction. Despite these findings, attempts to implement an X-walk correction were hindered by multiple complications, and CalCOS does not currently correct for this effect. One result of not applying an X-walk correction is

that data obtained near the end of operation at any lifetime position (i.e., at the lowest gain levels) suffer from distortions in the dispersion direction. Observations of ϵ Eri at LP3—obtained for the purpose of deriving dispersion solutions (Plesha et al. 2018)—show clear deviations from the expected linear dispersion solution, as demonstrated in Figure 4. By measuring and applying an X-walk correction, we will ensure that photons are assigned proper wavelength values regardless of the modal gain at which the observations were performed.

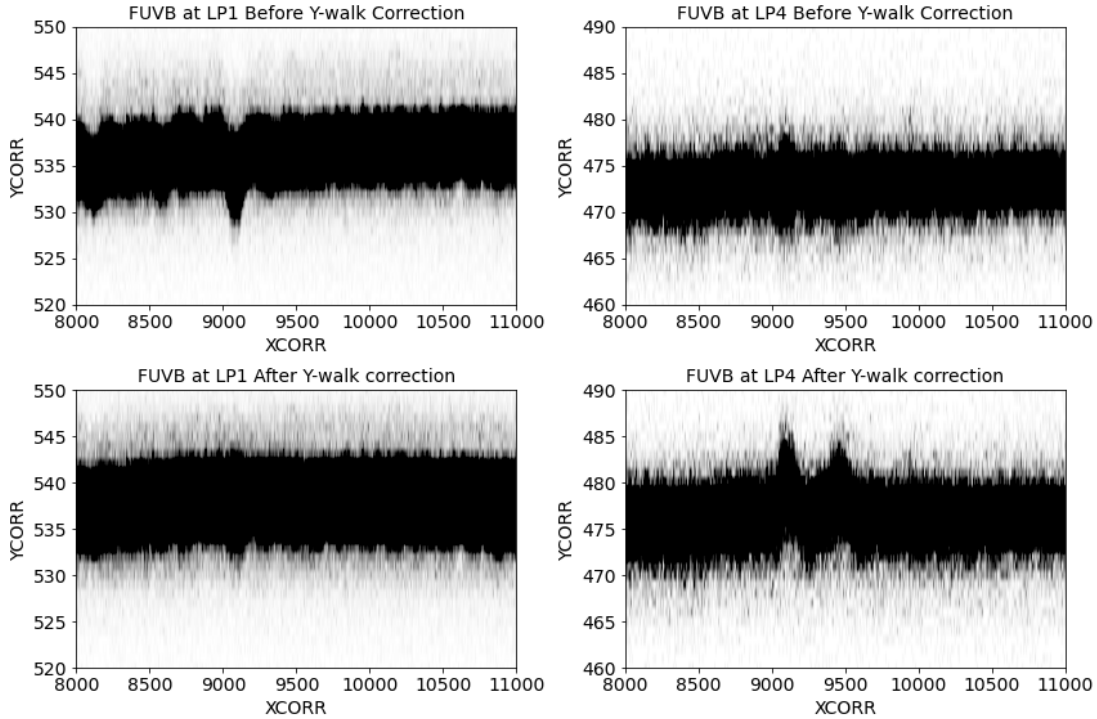


Figure 3. These images show the 2D spectral profiles for continuum observations at LP1 (left column; `lbo2hvljq`) and LP4 (right column; `lefe0lpxq`), before and after the existing Y-walk correction (`14o2013rlywalk.fits`) has been applied (top and bottom rows, respectively). The existing correction improves the shape of the spectral trace at LP1, but clearly distorts the trace at LP4, thus motivating a new y-dependent Y-walk correction (figure taken from Hasselquist et al. 2025b).

3. Procedures

3.1 Testing Metrics

To test for improvements to the geometric distortion and walk corrections, we make two assumptions regarding COS FUV data. First, the spectrum projected onto the detector

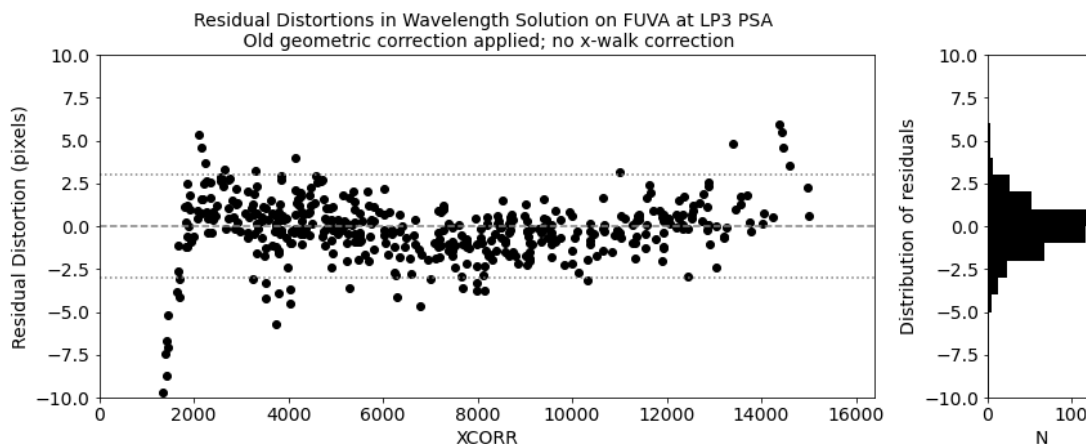


Figure 4. Residual shifts (in pixels) between the measured and predicted locations for emission lines in the spectrum of ϵ Eri observed on FUVa at LP3 (reanalysis of the data presented in Plesha et al. 2018). The large scale curvature represents a departure from the linear dispersion solutions, and is caused by X-walk. Large, negative residuals at the left edge are caused by the inadequate geometric distortion correction.

is straight and parallel to the dispersion axis. This means that spectra should be located at a constant y -location across the detector, and can be used to test corrections in the y direction. Second, dispersion solutions for all of the COS FUV medium resolution modes (G130M & G160M) are linear, i.e.,

$$\lambda = a_0 + a_1 \times \text{XFULL}. \quad (1)$$

By measuring the locations of features with known wavelengths on the detector and comparing those results to the predicted locations of those same features given a best-fit dispersion solution, we can test corrections in the x direction. Improved geometric distortion and X-walk corrections should both remove any coherent structures in a plot of residual shift vs. XCORR (e.g., Figures 1 and 4), and also narrow the width of the distribution of residual shifts. These metrics serve as our method for testing new reference files. A detailed description of the dispersion solution testing metrics can be found in French et al. (2025).

3.2 Workflow

The COS data that are used to derive the geometric distortion correction are not immune to walk, and vice versa. This complicates the overall analysis plan, as measurement of one effect without correcting for the other will produce a “correction” that has contributions from both. To separate the two effects to the greatest extent possible, the measurement of each, and the creation of new reference files was done iteratively, as follows:

1. Measure the geometric distortion using the geometric data set.
2. Create a geometric distortion correction reference file.
3. Apply the geometric distortion correction to the X-walk data set.
4. Measure the X-walk using the X-walk data set.
5. Create an X-walk correction reference file.
6. Apply the X-walk correction to the geometric data set.

By repeating this sequence, the effects of geometric distortion and walk can be separated, such that the geometric distortion correction does not incorrectly include walk effects, and the walk correction does not incorrectly include geometric distortion effects. Every time a new reference file was created, the full suite of testing metrics data was re-analyzed and the results were compared to those from the previous testing round to track improvements. The original plan was to declare the iterative procedure complete when the residuals from successive testing rounds showed insignificant further improvement, but this was abandoned for reasons discussed below in Section 3.6.

3.3 Geometric Distortion Measurement

Measurement of the geometric distortion requires a data set that covers as much of the detector as possible with features that appear at known *physical* locations on the detector. The physical location is used to determine the expected pixel values in a uniform array of digital pixels, and the difference between that predicted position and the measured position is the distortion. Initially, the COS FUV geometric distortion was measured using a uniformly illuminated pinhole mask (Béland et al. 2003), but due to partial disassembly of the detector this calibration became invalid (Béland & Penton 2006). The data set used to create the existing geometric distortion correction—and that we have used to re-measure the geometric distortion—is a series of 112 Pt-Ne emission line spectra taken at several cross-dispersion locations on the detector during thermal vacuum testing in 2003 (TV03). Measurement of the geometric distortion using these data, and creation of the new GEOFILE reference file are described in detail by Kakkad et al. (2025).

3.4 X-Walk Measurement

Measurement of X-walk requires a data set that is well-sampled in XCORR and obtained across a wide range of gain levels (i.e., well-sampled in PHA). For a feature that is projected onto the same location on the detector in multiple exposures taken at different gain levels, any shift of that feature in the x -direction between exposures is presumed to

be due to X-walk. The data set used to measure X-walk (PID 12793) consists of multiple series of Pt-Ne spectra, with each series taken at a single y -location on the detector, but at several different high voltages to sample different gain levels. Measurement of X-walk and creation of the new XWLKFILE reference file are described in detail by Hasselquist et al. (2025a).

3.5 Y-Walk Measurement

Measurement of Y-walk requires a data set that is well-sampled in YCORR and obtained across a wide range of gain levels. For a feature that is projected onto the same location on the detector in multiple exposures taken at different gain levels, any shift of that feature in the y -direction between exposures is presumed to be due to Y-walk. There is no uniform data set explicitly taken for the purpose of measuring Y-walk. Instead, we utilize a variety of observations that satisfy the “wide range of gain levels” criterion at different YCORR locations on the detector (e.g., geocoronal Ly- α emission on FUVB at LP4 and LP5; the X-walk data set on both segments at LP2; a hot spot on FUVB at LP4, etc.) to measure Y-walk at different y -locations. Measurement of Y-walk using the varied data sets and creation of the new YWLKFILE reference file are described in detail by Hasselquist et al. (2025b).

3.6 Delta Geometric Distortion Correction

Following two full rounds of iteratively measuring the geometric distortion and X-walk it became clear that there were coherent structures in the testing metrics wavelength residuals that were not being improved by either correction (see Figure 5). By performing the testing metrics analysis on the TV03 data used to measure the geometric distortion (which were taken at high gain) we determined that the coherent structures are not present in those data, and so cannot be removed by the geometric distortion correction. By performing the testing metrics analysis on the highest gain data (that serve as our reference data) from PID 12793 we determined that the coherent structures are present in those data, and so cannot be removed by the X-walk correction. The exact reason as to why the features do not appear in the high gain geometric distortion correction data set but do appear in the high gain X-walk data set is unknown⁴, but the result is a situation where further iteration cannot possibly remove the coherent structures from the testing metrics residuals.

In order to remove the coherent structures from the residuals we opted to utilize the delta-geometric correction step in CalCOS. This step performs a second, smaller geometric correction after the initial geometric distortion correction, and was originally introduced in 2017 with the intention of fixing the residual errors at LP4 shown in Figure 1. Due to complications that necessitated the full recalibration effort being described

⁴One speculation is a difference between data taken on the ground and on-orbit.

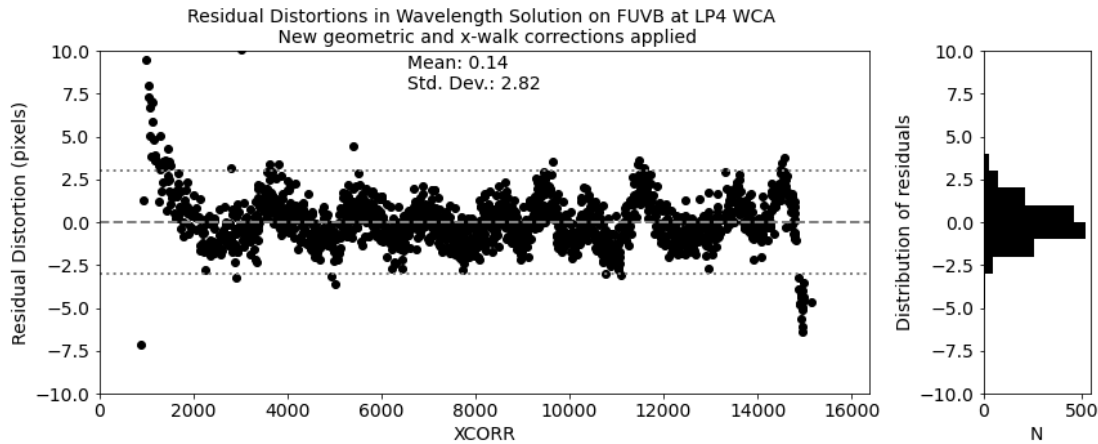


Figure 5. Residual shifts between measured and predicted locations for emission lines in spectra of the Pt-Ne hollow cathode lamp on the COS calibration platform, observed through the wavelength calibration aperture (WCA). Both the new geometric distortion and X-walk corrections have been applied, but a pattern of coherent structures is still clearly visible in the residuals (figure taken from Indriolo et al. 2025a).

here, the delta-geometric correction has remained unused⁵ until now. Measurement of the coherent structures uses the testing metrics residuals as input, and is described in Indriolo et al. (2025a), along with the method for creating a delta-geometric correction reference file from those measurements.

4. Summary

The result of the workflow described above is four new reference files (GEOFILE, DGEOFILE, XWLKFILE, YWLKFILE) to be used with CalCOS. A full series of plots made to test the performance of these new files is provided in French et al. (2025). Here, we simply revisit the motivation provided by Figures 1–4 in the corresponding Figures 6–9. Figure 6 demonstrates that the new geometric distortion correction is no longer introducing artifacts into the data, and the distribution of residuals (mean \pm standard deviation) on FUVB at LP4 is improved from -0.29 ± 2.46 to -0.11 ± 1.37 using the old and new geometric distortion corrections, respectively. Figure 7 shows that the new geometric distortion correction has also successfully removed the grid wire impostors from FUVB. Figure 8 shows that the new Y-walk is equivalent to the old Y-walk at LP1, but makes a significant improvement at LP4. In simultaneously removing the effects of Y-walk at both LP1 and LP4, the new y-dependent Y-walk correction is working as intended. Figure 9 shows that the new X-walk correction

⁵Image arrays in the existing DGEOFILE reference file are full of zeros, and so do not move photon events.

reduces residual distortions for data taken at low gain. Finally, Figure 10 shows that the magnitude of the coherent structures seen in the residuals is reduced when the new delta-geometric correction is applied, with the width of the distribution of residuals dropping from $\sigma = 2.82$ to $\sigma = 2.62$ pixels. Together, these results demonstrate that the new geometric distortion, delta-geometric, and walk corrections substantially improve COS data products by successfully addressing the issues that motivated this project.

For the interested reader, a summary of this project was also presented at the 2024 Winter AAS meeting as an iposter (Indriolo et al. 2024), which can be accessed online.⁶

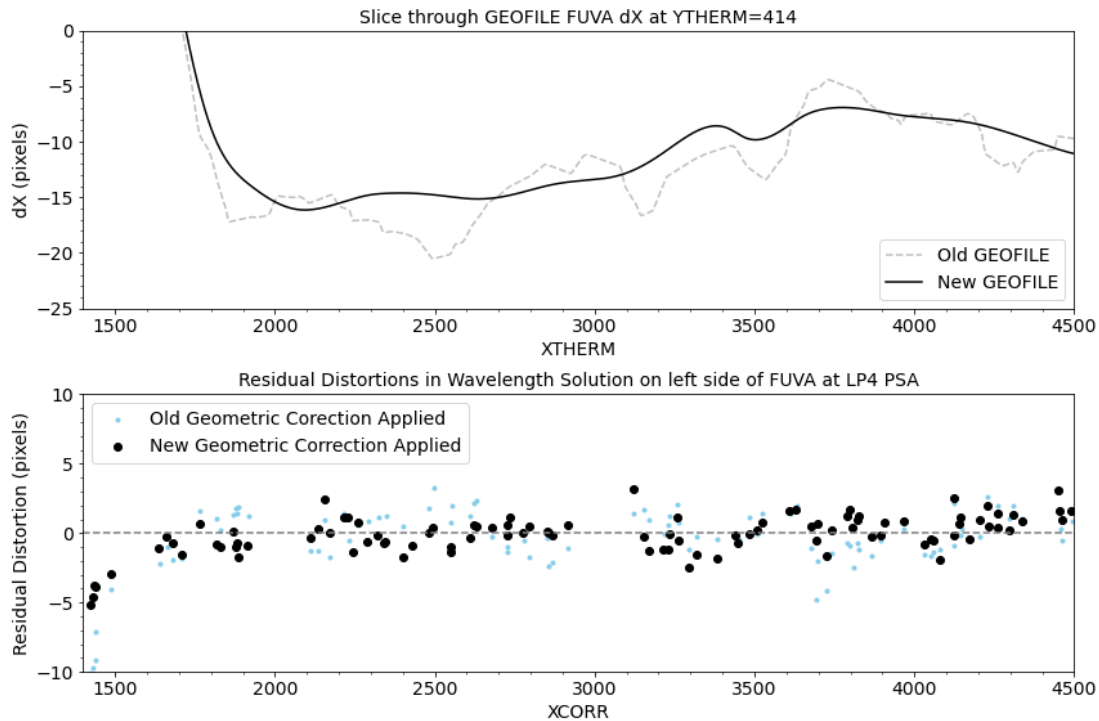


Figure 6. Companion to Figure 1, now comparing new and old results. In the top panel the black curve is a slice through the new FUVA dx geometric distortion correction at YTHERM=414, while the dashed grey curve is the same slice through the old GEOFILE. In the bottom panel the black points show the residual shifts after application of the new geometric distortion correction, while light blue dots show the residual shifts from the same data set when the old geometric distortion correction was applied. The strong correlation between the old dx correction and residual distortions has been removed (e.g., near XCORR=2500 and XCORR=3700), so we are confident that the geometric distortion correction is no longer introducing artifacts in the calibrated data.

⁶<https://aas243-aas.ipostersessions.com/default.aspx?s=FF-40-8B-EA-0D-CE-7E-B9-6E-E1-D6-F3-C8-7B-BC-AD&guestview=true>

5. Future Work

The geometric distortion and walk corrections occur early within the flow of calibration steps applied by CalCOS. They are responsible for moving photons to “corrected” locations prior to calibration steps that begin to analyze the data and extract spectra. This means that any “downstream” reference files with a dependence on detector position will be altered by the application of different geometric distortion and walk corrections. As such, the new geometric distortion, delta-geometric, X-walk, and Y-walk reference files necessitate the rederivation of all reference files with positional or wavelength dependencies (BRFTAB, SPOTTAB, GSAGTAB, BPIXTAB, XTRACTAB, TWOZXTAB, PROFTAB, TRACETAB, LAMPTAB, DISPTAB, FLATFILE, FLUXTAB, and TDSTAB). Only after the creation of new versions of all of these reference files will the benefits of the new geometric distortion and walk corrections be available within CalCOS. A summary of this effort is described in Indriolo et al. (2025b), with more specific details documented in references therein.

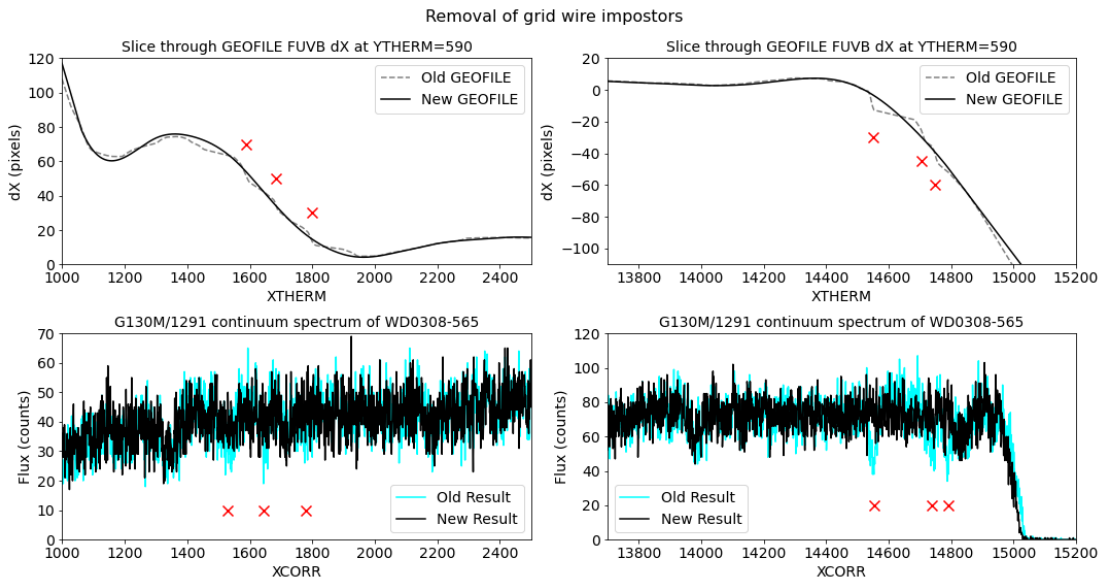


Figure 7. Companion to Figure 2, now showing results with the grid wire impostors removed. In the top panels, black curves show slices through the newly derived FUVB dx geometric distortion correction, while dashed grey lines show slices through the old correction. Red crosses mark the features giving rise to grid wire impostors in the old reference file, and it is clear these have been eliminated in the new reference file. The results of processing data with the new correction are shown as black curves in the bottom panels, while data processed with the old correction are shown in cyan. The flux deficits caused by the grid wire impostors have been removed. As a result of this improvement, the grid wire impostor features will be removed from all FUVB flat field reference files (figure taken from Kakkad et al. 2025.).

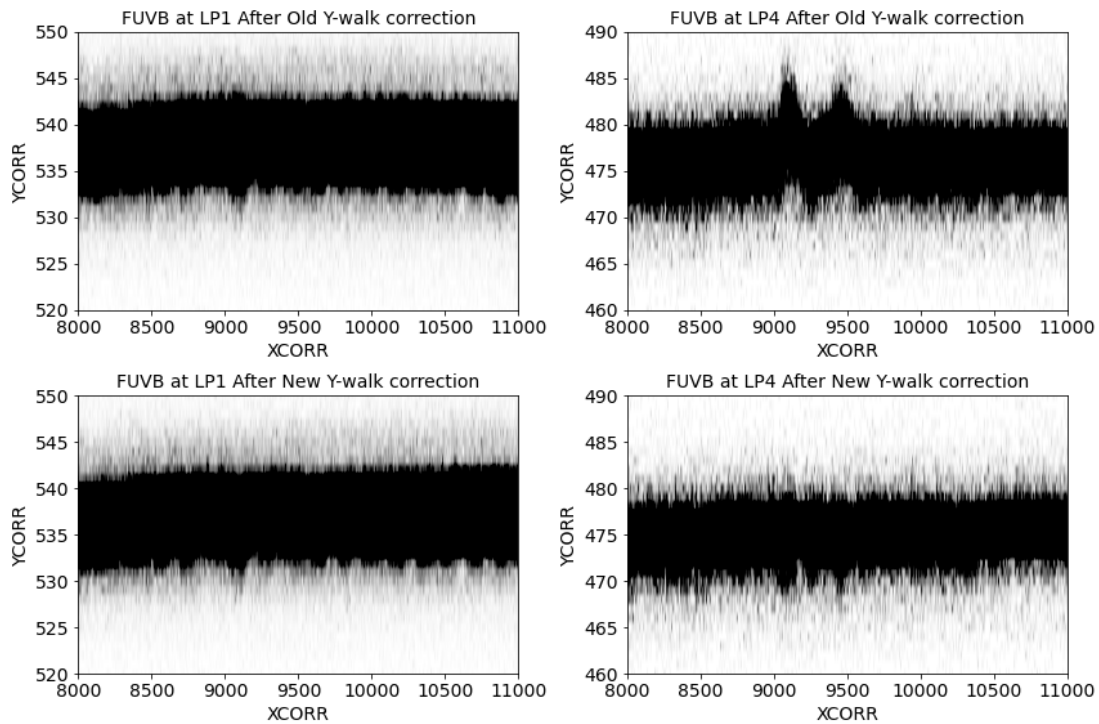


Figure 8. Companion to Figure 3, with the top row now showing 2D spectral profiles with the old Y-walk correction applied, while the bottom row shows profiles with the newly derived y-dependent Y-walk correction applied. Data at both LP1 and LP4 are now properly corrected for Y-walk (figure taken from Hasselquist et al. 2025b).

Acknowledgements

The authors would like to acknowledge S. V. Penton, J. White, and D. Dashtamirova for their contributions to this effort while working at STScI.

Change History for COS ISR 2025-07

Version 1: 2 July 2025- Original Document

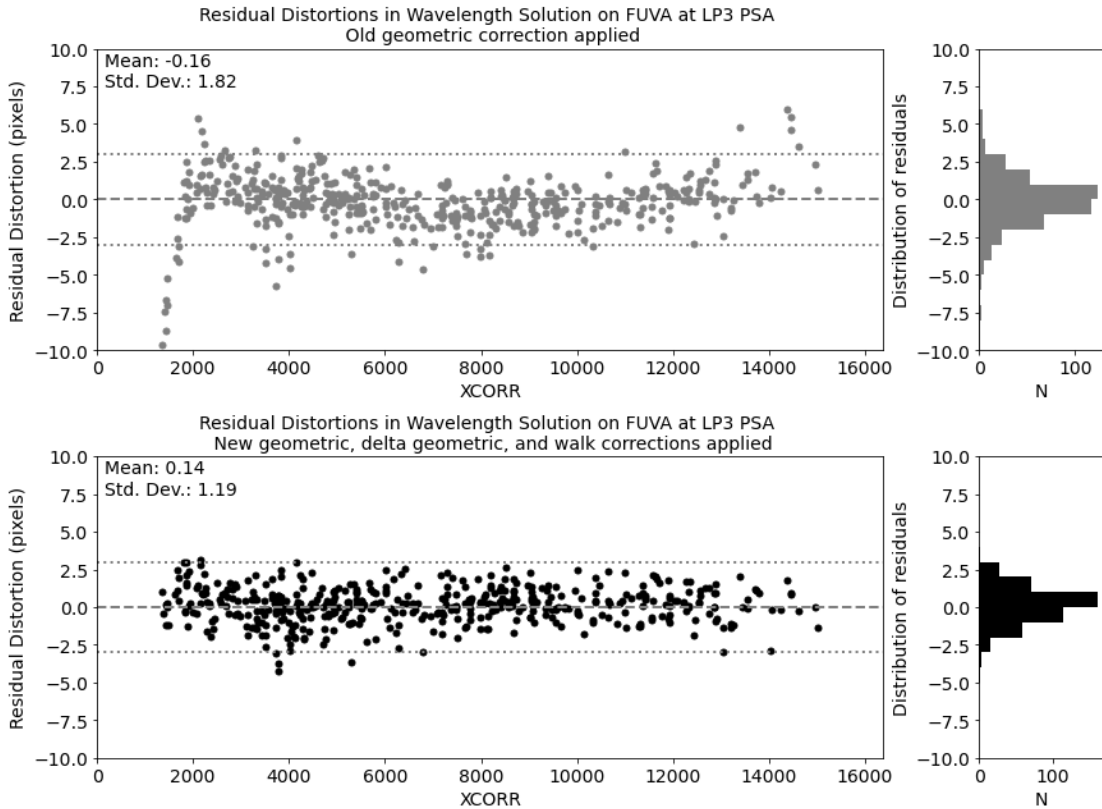


Figure 9. Companion to Figure 4, now showing residual distortions for data with the old geometric distortion correction applied (top panel) and for data with the new geometric, delta-geometric, and X-walk corrections applied (bottom panel). Both the large scale curvature due to X-walk and the large residuals at the edge of the detector due to geometric distortion have been removed.

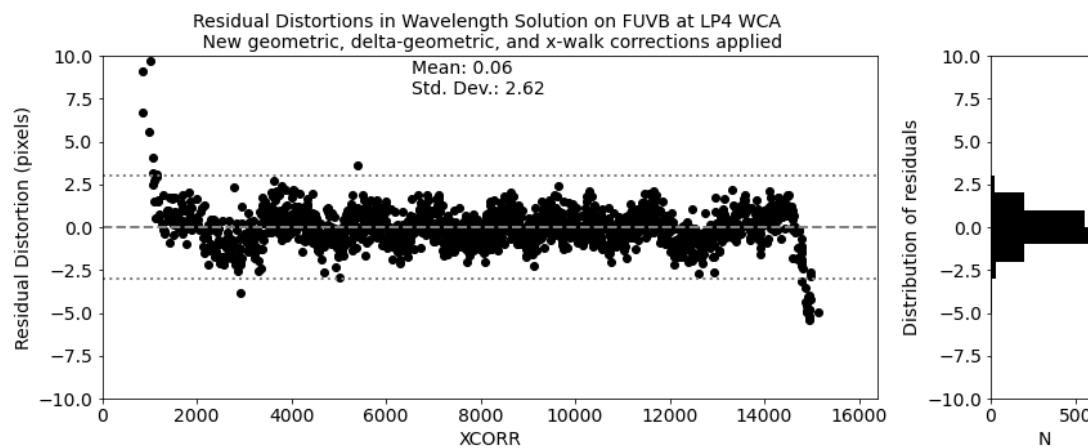


Figure 10. Companion to Figure 5, now with the new delta-geometric correction applied as well. The magnitude of the coherent structures in the residuals has been greatly reduced, although they are not fully removed for reasons discussed in Indriolo et al. (2025a), from which this figure was taken.

References

- Béland, S., et al. 2003, TER COS-11-0044, *COS FUV Detector Geometric Distortion Maps*
- Béland, S. & Penton, S. V. 2006, ADASS 351, 339, *Correcting for the Geometric Distortions on the COS FUV Detector*
- French, D., et al. 2025, COS ISR 2025-xx *Testing metrics* (In Preparation)
- Hasselquist, S., et al. 2025, COS ISR 2025-10, *Determining X-Walk Corrections for the COS FUV Detector*
- Hasselquist, S., et al. 2025, COS ISR 2025-11, *Determining Y-Walk Corrections for the COS FUV Detector*
- Hirschauer, A. S., et al. 2024, *Cosmic Origins Spectrograph Instrument Handbook*, Version 17.0 (Baltimore: STScI)
- Indriolo, N., et al. 2024 AAS Meeting #243, id. 360.07 *Improvements to the COS FUV Geometric Distortion and Walk Corrections*
- Indriolo, N., et al. 2025a, COS ISR 2025-08, *Measurement and Implementation of a Delta-Geometric Correction for the COS FUV Detector*
- Indriolo, N., et al. 2025b, COS ISR 2025-xx, *Reference File Updates Following the Application of New Geometric Distortion and Walk Corrections I: Overview* (In Preparation)
- Kakkad, D., et al. 2025, COS ISR 2025-09, *A Revised Geometric Distortion Correction for the Far-Ultraviolet Detector of the Cosmic Origins Spectrograph*
- Osten, R., et al. 2013, COS ISR 2013-16, *Summary of Results from the First Move to a New COS FUV Lifetime Position*
- Plesha, R., et al. 2018, COS ISR 2018-24, *Improvements to the COS FUV G130M and G160M Wavelength Solutions at Lifetime Position 3*
- Sahnow, D. J., Oliveira, C., Aloisi, A., et al. 2011, Proc. SPIE 8145, 81450Q-1, *Gain sag in the FUV detector of the Cosmic Origins Spectrograph*
- Sahnow, D. J., Penton, S., Ake, T., et al. 2016, Proc. SPIE 9905, 99052T-1, *Correcting for errors due to walk and geometric distortion in the COS FUV detector*
- Sahnow, D. J. 2018, COS TIR 2018-03, *Using the FENA1 Data for Measuring Walk on the COS FUV Detector*
- Soderblom, D., et al. 2022, *COS Data Handbook*, Version 5.1, (Baltimore: STScI).
- Vallerga, J. V. & McPhate, J. B. 2000, Proc. SPIE 4139, *Optimization of the readout electronics for microchannel plate delay line anodes*
- Vallerga, J. V., McPhate, J. B., Martin, A. P., et al. 2001, Proc. SPIE 4498, 141, *HST-COS far ultraviolet detector: final ground calibration*
- Wilkinson, E., Penton, S., Beland, S., et al. 2001, Proc. SPIE 4498, 267, *Algorithms for correcting geometric distortions in delay line anodes*